



**HAL**  
open science

## Measurements of HNO<sub>3</sub> and N<sub>2</sub>O<sub>5</sub> using Ion drift ? Chemical Ionization Mass Spectrometry during the MCMA ? 2006 Campaign

J. Zheng, R. Zhang, E. C. Fortner, L. Molina, A. C. Aiken, J. L. Jimenez, K.  
Gäggeler, J. Dommen, S. Dusanter, P. S . Stevens, et al.

► **To cite this version:**

J. Zheng, R. Zhang, E. C. Fortner, L. Molina, A. C. Aiken, et al.. Measurements of HNO<sub>3</sub> and N<sub>2</sub>O<sub>5</sub> using Ion drift ? Chemical Ionization Mass Spectrometry during the MCMA ? 2006 Campaign. Atmospheric Chemistry and Physics Discussions, 2008, 8 (2), pp.4877-4909. hal-00304024

**HAL Id: hal-00304024**

**<https://hal.science/hal-00304024>**

Submitted on 18 Jun 2008

**HAL** is a multi-disciplinary open access archive for the deposit and dissemination of scientific research documents, whether they are published or not. The documents may come from teaching and research institutions in France or abroad, or from public or private research centers.

L'archive ouverte pluridisciplinaire **HAL**, est destinée au dépôt et à la diffusion de documents scientifiques de niveau recherche, publiés ou non, émanant des établissements d'enseignement et de recherche français ou étrangers, des laboratoires publics ou privés.

# Measurements of HNO<sub>3</sub> and N<sub>2</sub>O<sub>5</sub> using Ion drift – Chemical Ionization Mass Spectrometry during the MCMA – 2006 Campaign

J. Zheng<sup>1</sup>, R. Zhang<sup>1</sup>, E. C. Fortner<sup>1,\*</sup>, L. Molina<sup>2</sup>, A. C. Aiken<sup>3</sup>, J. L. Jimenez<sup>3</sup>,  
K. Gäggeler<sup>4</sup>, J. Dommen<sup>4</sup>, S. Dusanter<sup>5</sup>, P. S. Stevens<sup>5</sup>, and X. Tie<sup>6</sup>

<sup>1</sup>Dept. Atmospheric Sciences, Texas A & M University, College Station, Texas 77843, TX, USA

<sup>2</sup>Molina Center for Energy and the Environment, La Jolla, CA, USA

<sup>3</sup>Dept. Chemistry and Biochemistry, University of Colorado, Boulder, CO, USA

<sup>4</sup>Laboratory of Atmospheric Chemistry, Paul Scherrer Institute, 5232 Villigen, Switzerland

<sup>5</sup>Dept. Chemistry, Indiana University, Bloomington, IN, USA

<sup>6</sup>Atmospheric Chemistry Division, National Center for Atmospheric Research, Boulder, CO, USA

\*now at: Dept. Chemistry and Biochemistry, Montana State University, Bozeman, MT, USA

Received: 18 January 2008 – Accepted: 22 January 2008 – Published: 6 March 2008

Correspondence to: R. Zhang (zhang@ariel.met.tamu.edu)

Published by Copernicus Publications on behalf of the European Geosciences Union.

Nitric acid during  
MCMA 2006

R. Zhang et al.

Title Page

Abstract

Introduction

Conclusions

References

Tables

Figures

◀

▶

◀

▶

Back

Close

Full Screen / Esc

Printer-friendly Version

Interactive Discussion



## Abstract

An ion drift – chemical ionization mass spectrometry (ID-CIMS) was deployed in Mexico City between 5 and 31 March to measure  $\text{HNO}_3$  and  $\text{N}_2\text{O}_5$  during the 2006 Mexico City Metropolitan Area (MCMA) field campaign. The observation site, T0, was located at the Instituto Mexicano del Petróleo at the center of the Mexico City Basin with major emissions of pollutants from both domestic and industrial sources. Diurnally,  $\text{HNO}_3$  was less than 200 parts per trillion (ppt) during the night and in the early morning, increased steadily from around 09:00 a.m. central standard time (CST), reached a peak value of 0.5 to 3 parts per billion (ppb) in the early afternoon, and declined sharply to less than half of the peak value near 05:00 p.m. CST. An inter-comparison between the ID-CIMS and an ion chromatograph/mass spectrometer (ICMS) showed a good correlation in the  $\text{HNO}_3$  measurements ( $R^2=0.75$ ). The  $\text{HNO}_3$  mixing ratio was found to anti-correlate with aerosol nitrate, suggesting that the gaseous  $\text{HNO}_3$  concentration was controlled by the gas-particle partitioning process. During most times of the MCMA 2006 field campaign,  $\text{N}_2\text{O}_5$  was found to be under the detection limit (about 20 ppt for a 10 s integration time) of the ID-CIMS, because of high NO mixing ratio ( $>100$  ppb) during the night. With one exception on 26 March 2006, about 40 ppt  $\text{N}_2\text{O}_5$  was observed during the late afternoon and early evening hours under a cloudy condition, before NO built up at the surface site. The results revealed that during the 2006 MCMA field campaign  $\text{HNO}_3$  was primarily produced by the reaction of OH with  $\text{NO}_2$  and regulated by gas/particle partitioning, and  $\text{HNO}_3$  production from  $\text{N}_2\text{O}_5$  hydrolysis during the nighttime was small because of high NO and low  $\text{O}_3$  concentrations near the surface.

## 1 Introduction

For decades, the Mexico City Metropolitan Area (MCMA), the biggest megacity in the world, has suffered from severe air pollution, especially in ozone ( $\text{O}_3$ ) and particu-

## Nitric acid during MCMA 2006

R. Zhang et al.

Title Page

Abstract

Introduction

Conclusions

References

Tables

Figures

◀

▶

◀

▶

Back

Close

Full Screen / Esc

Printer-friendly Version

Interactive Discussion



**Nitric acid during  
MCMA 2006**

R. Zhang et al.

Title Page

Abstract

Introduction

Conclusions

References

Tables

Figures

◀

▶

◀

▶

Back

Close

Full Screen / Esc

Printer-friendly Version

Interactive Discussion



late matter (Molina and Molina, 2002; Molina et al., 2007). As the home of 20 million residents, 3.5 million vehicles, and 35 000 industries, the MCMA emits annually near 206 kilotons of nitrogen oxides ( $\text{NO}_x = \text{NO} + \text{NO}_2$ ), 22.5 kilotons of sulfur dioxide ( $\text{SO}_2$ ), and 1769 kilotons of volatile organic compounds (VOCs) (Molina and Molina, 2002) into the atmosphere, due to both domestic and industrial fossil fuel consump-  
5 tions. Furthermore, the unique combination of geographical conditions, i.e. the basin topography, tropical solar radiation ( $19^\circ 25' \text{N}$  and  $99^\circ 10' \text{W}$ ), and high elevation (2240 m a.m.s.l.), makes air pollutants easier to accumulate in the MCMA and is favorable for photochemical production of  $\text{O}_3$  and aerosols (Molina and Molina, 2002; Zhang et al., 2004a). Since 1988, this region annually experiences an hourly average  $\text{O}_3$  concentra-  
10 tion higher than 110 ppb for over 80% days and a peak  $\text{O}_3$  concentration of frequently more than 300 ppb (Molina and Molina, 2002). Both VOCs and  $\text{NO}_x$  play critical roles during  $\text{O}_3$  formation in the troposphere (Finlayson-Pitts and Pitts, 1999) and the variations in their concentrations and the ensuing effects on  $\text{O}_3$  production rate can be  
15 characterized as either  $\text{NO}_x$ -sensitive or VOC-sensitive (Sillman, 1999; Lei et al., 2004; Zhang et al., 2004b). Recently, based on a model study, Tie et al. (2007) suggested that the  $\text{O}_3$  formation in the MCMA was VOC-limited. The lifecycle of  $\text{NO}_x$  and its budget in the MCMA is one of the critical pre-required information to develop effective  $\text{O}_3$  control strategies (Lei et al., 2007). The dominant daytime sink of  $\text{NO}_x$  is through the  
20 oxidation of  $\text{NO}_2$  by the hydroxyl radical (OH) to form nitric acid ( $\text{HNO}_3$ ),



which is removed from the atmosphere by dry and wet depositions (Finlayson-Pitts and Pitts, 1999). Generally,  $\text{HNO}_3$  deposition is considered as an irreversible sink for  $\text{NO}_x$ , but recent studies have suggested that  $\text{HNO}_3$  deposited on the surface can be recycled  
25 back into the atmosphere as  $\text{NO}_x$  by heterogeneous reactions with NO (Saliba et al., 2001) and photolysis in the presence of water (Ramazan et al., 2006). Under certain meteorological conditions,  $\text{HNO}_3$  can be transported over 1000 km downwind from the plume origin, and a  $\text{HNO}_3$  enriched plume can potentially contribute to  $\text{O}_3$  production far away from its origin.

During the nighttime,  $\text{NO}_x$  will titrate  $\text{O}_3$  to form the nitrate radical ( $\text{NO}_3$ ),



which can further react reversibly with  $\text{NO}_2$  to form dinitrogen pentoxide ( $\text{N}_2\text{O}_5$ ) (for Reaction 4,  $K_{eq} = 4.5 \times 10^{-14} \exp[-1260/T] \text{ cm}^3 \text{ molecule}^{-1} \text{ s}^{-1}$ , JPL, 2006). At night,  $\text{NO}_3$  can exist in significant concentrations and undergo H-atom abstraction or addition reactions with hydrocarbons in a similar way as OH radicals during daytime (Suh et al., 2001). Comparing with  $\text{NO}_3$ ,  $\text{N}_2\text{O}_5$  is relatively unreactive, but it can act as a reservoir of  $\text{NO}_3$  and undergo heterogeneous hydrolysis to form  $\text{HNO}_3$  (Zhang et al., 1995; Brown et al., 2006). Therefore, in-situ observations of  $\text{HNO}_3$  and  $\text{N}_2\text{O}_5$  are indispensable to fully characterize the  $\text{NO}_x$  chemistry and budget in the troposphere and to develop effective control strategies.

Several measurement techniques have been developed to measure gaseous  $\text{HNO}_3$  in the troposphere, including a nylon filter (Anlauf et al., 1988), a mist chamber (Talbot et al., 1990), a denuder technique (Perrino et al., 1990; Simon et al., 1995), a luminol method (Hering et al., 1988), and chemical ionization mass spectrometry (CIMS) (Huey et al., 1998). Among the different approaches, the CIMS technique has the advantages of high sensitivity and fast time-response. Ambient  $\text{HNO}_3$  mixing ratio varies considerably temporally and spatially, with the reported values ranging from a few tens of ppt in clean remote environment to tens of ppb in aged urban plumes (Furutani and Akimoto, 2002; Huey et al., 2004). Despite the importance of  $\text{N}_2\text{O}_5$  in the nocturnal  $\text{NO}_x$  chemistry, only recently in situ  $\text{N}_2\text{O}_5$  measurements have become possible. In situ measurements of  $\text{N}_2\text{O}_5$  have been performed by a cavity ring-down spectroscopy technique (CRDS) (Brown et al., 2002) and a CIMS technique (Huey et al., 1995). The

[Title Page](#)[Abstract](#)[Introduction](#)[Conclusions](#)[References](#)[Tables](#)[Figures](#)[◀](#)[▶](#)[◀](#)[▶](#)[Back](#)[Close](#)[Full Screen / Esc](#)[Printer-friendly Version](#)[Interactive Discussion](#)

observed  $\text{N}_2\text{O}_5$  concentration ranges from a few ppt to hundreds of ppt (Brown et al., 2001; 2006; Slusher et al., 2004).

A series of field campaigns have been conducted MCMA such as the 2002, 2003 and 2006 field campaigns. The objectives of these campaigns are to fully characterize the up-to-date air quality, to investigate the underline chemical processes that are responsible for secondary air pollutants formations, and to develop effective control strategies. In this paper, we present measurements of  $\text{HNO}_3$  and  $\text{N}_2\text{O}_5$  during the MCMA 2006 campaign from a recently developed ion drift-chemical ionization mass spectrometry (ID-CIMS) technique and its first field deployment. The results provide insights into the production and gas/particle partitioning of  $\text{HNO}_3$  in MCMA.

## 2 Experimental

### 2.1 ID-CIMS

The ID-CIMS method has been previously described (Fortner et al., 2004), and only details pertinent to this work are provided. Figure 1 shows a schematic diagram of the ID-CIMS that consists of an ion-drift tube, an ion source, and a quadrupole mass spectrometer. Also depicted in Fig. 1 is the  $\text{HNO}_3$  calibration device, which consists of a U-shape 1-inch outer diameter (OD) and 7-inch long glass tube wrapped with a temperature-regulated heating jacket (the dashed line). The U-tube has two symmetrical compartments divided by a glass grid in the middle, with one side housing a 5.0-cm long Teflon permeation tube (VICI Metronics Inc.) and the other filled with 0.5-cm diameter glass beads. A corona discharge is used to produce the ion source; it consists of a stainless steel needle typically biased by about  $-1200$  volts ( $V_1$ ) and a grounded  $1/4$ " OD stainless steel tube. A dry scroll pump (Varian) with a 500 liter per minute pumping speed draws the ambient air into the ID-CIMS system. A small portion of the air is introduced into the drift region through an orifice of about 0.5 mm. Within the drift tube, the reagent ion is produced and the ion-molecule reaction occurs to ionize

Title Page

Abstract

Introduction

Conclusions

References

Tables

Figures

◀

▶

◀

▶

Back

Close

Full Screen / Esc

Printer-friendly Version

Interactive Discussion



**Nitric acid during  
MCMA 2006**

R. Zhang et al.

Title Page

Abstract

Introduction

Conclusions

References

Tables

Figures

◀

▶

◀

▶

Back

Close

Full Screen / Esc

Printer-friendly Version

Interactive Discussion



the neutral species. The ion-drift tube is pumped by an Edwards E2M30 pump. A 10-ring drift tube sealed inside a heavy wall glass tube is used to guide the reagent ions and to control the ion-molecule reaction time. Each stainless steel ring is 7 mm thick and 40 mm OD and has a 14 mm diameter center hole. The rings are connected in series by three Teflon rods and isolated by 1/8" Nylon spacers. Neighboring rings are connected by a  $1.0 \pm 5\%$  M $\Omega$  resistor. A negative voltage is typically set to develop an electronic field in the drift tube (V2). The reagent and product ions are introduced to the MS system through a pinhole of 400  $\mu\text{m}$ , which is also biased negatively (V3). An Extrel 150-QS mass spectrometer is controlled by the Merlin 3.0 software (Extrel). Two high vacuum stages housing the quadrupole and the electron multiplier are pumped by two Varian TV-551 turbo molecular pumps with a Varian DS402 backing pump. During measurements, the dry scroll pump draws a flow of 200 standard liters per minute (slpm) ambient air into the inlet and only one liter air sample is sucked into the drift tube through the front orifice. A N<sub>2</sub> flow carrying the reagent ions is mixed with the air sample inside the drift tube and the ion-molecule reaction proceeds throughout the drift region. The typical pressure inside the drift tube is 2.8 torr. The reagent and the product ions are analyzed by the quadrupole mass spectrometer.

The unique character of the ID-CIMS lies in that it enables quantifications of neutral species by controlling the ion-molecule reaction time ( $\Delta t$ ),



where A corresponds to the neutral species to be analyzed and quantified, R represents the reagent ion,  $k$  is the reaction rate constant, and P denotes the product ion. The concentration of the neutral species after the reaction time  $\Delta t$  is expressed,

$$[\text{A}] = \frac{[\text{P}^{(+\text{or}-)}]}{k \Delta t [\text{R}^{(+\text{or}-)}]} \quad (7)$$

where  $[\text{P}^{(+\text{or}-)}]$  and  $[\text{R}^{(+\text{or}-)}]$  correspond to the intensities of product and reagent ions measured by the mass spectrometer, respectively.  $k$  can be obtained by laboratory

measurements or theoretical calculations (Zhao et al., 2004).  $\Delta t$  is determined by the length of the drift tube and the velocity of the reagent ions,  $U$ . While moving along the drift region with the carrier gas at a flow velocity of ( $U_f$ ), ions are also driven by a controllable electronic field to achieve a drift velocity ( $U_d$ ), which is determined by

$$U_d = \mu E \quad (8)$$

where  $\mu$  is the ionic mobility and  $E$  is the electronic field intensity.  $\mu$  can be calculated from the reduced ionic mobility,  $\mu_0$ ,

$$\mu = \mu_0(760/p)(T/273.16) \quad (9)$$

where  $p$  and  $T$  are the pressure and temperature inside the drift tube, respectively.

## 2.2 Ion chemistry

The ion chemistry used to detect  $\text{HNO}_3$  is similarly to that described by Huey and Lovejoy (1996). The reagent ion,  $\text{SiF}_6^-$ , is produced in two steps. A flow of about 300 standard cubic centimeters per minute (sccm)  $\text{N}_2$  doped with <0.1%  $\text{SF}_6$  flows through the ion source region, where  $\text{SF}_6$  is attached by one electron,



A trace amount of  $\text{SiF}_4$  is introduced downstream of the ion source and reacts with  $\text{SF}_6^-$  through a fluoride transfer reaction to produce  $\text{SiF}_5^-$ .  $\text{SiF}_5^-$  subsequently reacts with  $\text{HNO}_3$  at a rate of  $(3.8 \pm 1) \times 10^{-10} \text{ cm}^3 \text{ molecule}^{-1} \text{ s}^{-1}$  (Huey and Lovejoy, 1996) to form  $\text{SiF}_5^- \cdot \text{HNO}_3$  adduct. During the field campaign, both the isotope peak of the reagent ion ( $^{30}\text{SiF}_5^-$ ,  $m/e=125$ ) and the product ion,  $\text{SiF}_5^- \cdot \text{HNO}_3$  ( $m/e=186$ ) are recorded continuously.

Title Page

Abstract

Introduction

Conclusions

References

Tables

Figures

◀

▶

◀

▶

Back

Close

Full Screen / Esc

Printer-friendly Version

Interactive Discussion



$\text{N}_2\text{O}_5$  is detected as the  $\text{I}^-$  reagent ion, which is generated inside the ion source through electron attachment reaction,



$\text{N}_2\text{O}_5$  subsequently reacts with  $\text{I}^-$  to produce  $\text{NO}_3^-$ , with a rate constant of  $1.3 \times 10^{-9} \text{ cm}^3 \text{ molecule}^{-1} \text{ s}^{-1}$  (Huey et al., 1995).

The reduced ionic mobility  $\mu_0$  of  $\text{SiF}_5^-$  and  $\text{I}^-$  are determined according to Mason and McDaniel (1988),

$$\mu_0 = \frac{1.85 \times 10^4}{\bar{\Omega} \sqrt{T_{\text{eff}}}} \left( \frac{m+M}{mM} \right)^{1/2} \text{ cm}^2 \cdot \text{V}^{-1} \cdot \text{s}^{-1}, \quad (15)$$

where  $T_{\text{eff}}$  is the effective temperature of the carrier gas (in K),  $m$  and  $M$  are the masses (in atomic mass units) of the ion ( $\text{SiF}_5^-$  or  $\text{I}^-$ ) and the carrier gas ( $\text{N}_2$ ), respectively, and  $\bar{\Omega}$  is the momentum-transfer collision integral (in  $\text{cm}^2$ ).  $T_{\text{eff}}$  is given by

$$\frac{3}{2} k_b T_{\text{eff}} = \frac{3}{2} k_b T + \frac{1}{2} m U_f^2 \quad (16)$$

where  $k_b$  is Boltzmann's constant and  $T$  is the temperature of the carrier gas.  $\bar{\Omega}$  is obtained from the tabulated values (Viehland et al., 1975) based on ion-neutral interaction potentials. Because no experimental data are available to characterize the ion-neutral interactions in the  $\text{SiF}_5^-/\text{N}_2$  or  $\text{I}^-/\text{N}_2$  system, we perform ab initio calculations to obtain the ion-neutral interaction potentials using the Gaussian 03 software package on an SGI Origin 3800 supercomputer (Lei et al., 2000; Lei and Zhang, 2001). The geometry optimization and energy calculations at a series of center-to-center distances for  $\text{SiF}_5^-/\text{N}_2$  and  $\text{I}^-/\text{N}_2$  systems are conducted using density function method B3LYP/6-

[Title Page](#)[Abstract](#)[Introduction](#)[Conclusions](#)[References](#)[Tables](#)[Figures](#)[◀](#)[▶](#)[◀](#)[▶](#)[Back](#)[Close](#)[Full Screen / Esc](#)[Printer-friendly Version](#)[Interactive Discussion](#)

31G(d,p) and B3LYP/LANL2DZ, respectively. The results are then fitted with a potential model

$$V(r) = \frac{B}{r^{12}} - \frac{C_6}{r^6} - \frac{C_4}{r^4} \quad (17)$$

where the  $B$  term represents the short-range repulsion energy,  $C_6$  denotes the charge-induced quadrupole attraction plus the London dispersion attraction, and  $C_4$  represents the attraction between the ion and the dipole induced in  $N_2$ . Based on the calculated potential well depth,  $\varepsilon$ , and the minimum position,  $r_m$ , the corresponding value of  $\bar{Q}$  is obtained. Table 1 provides a summary of the calculations. The predicted values of  $\mu_0$  for  $SiF_5^-$  and  $I^-$  are  $1.89$  and  $2.09 \text{ cm}^2 \cdot \text{V}^{-1} \cdot \text{s}^{-1}$ , respectively.

### 2.3 Instrument calibrations

The ID-CIMS, in principle, can quantitatively determine the concentration of neutral species using Eq. (7). The accuracy of the calculation is affected by uncertainties associated with several parameters, including the reduced ionic mobility, the ion-molecule reaction rate constants, the transmission efficiencies of the quadrupole mass filter, fragmentation in the ion-molecule reaction, and etc. These parameters are invariant under given experimental conditions and their uncertainties are minimized by calibration with known concentration gas standards.

The  $HNO_3$  calibration employs a permeation device, as shown in Fig. 1. The permeation device (Fig. 1a) is heated and maintained at  $40.0^\circ\text{C}$ . About 400 to 500 sccm  $N_2$  carrier gas is fed into the side filled with glass beads and warmed to the same temperature as the entire device before entering the permeation tube side. After the permeation device, the concentrated  $HNO_3/N_2$  stream is injected into a 1-inch OD Teflon tube in which they are mixed with a 20 to 150 slpm dilution flow. The concentrations of the exiting  $HNO_3$  flow ranges between 0.25 and 2 ppb. Prior to each calibration, the permeation device is maintained at an operational condition for more than 6 h to achieve equilibrium.

Title Page

Abstract

Introduction

Conclusions

References

Tables

Figures

◀

▶

◀

▶

Back

Close

Full Screen / Esc

Printer-friendly Version

Interactive Discussion



**Nitric acid during  
MCMA 2006**

R. Zhang et al.

Due to the “sticky” nature of  $\text{HNO}_3$ , it is necessary to verify the effective permeation rate under the normal operation condition to account for any possible wall loss during the preparation of the calibration standards. The procedure to verify the permeation rate is similar to the calibration process, but, instead of introducing the  $\text{HNO}_3$  standards into the ID-CIMS for calibration, the  $\text{HNO}_3$  standard is introduced to a glass bubbler containing a specific amount of pure water ( $R > 17 \text{ M}\Omega$ ) for a specific time. All tubing is passivated by the  $\text{HNO}_3$  standard for a few hours before the final solution is collected. The  $\text{HNO}_3$  solution is analyzed by ion chromatography (DIONEX), which is calibrated by ultra pure sodium nitrate (Sigma-Aldrich) solutions. The measured permeation rate is  $109 \pm 1.2 \text{ ng/min}$ , within 10% of the manufacture certified value ( $116 \text{ ng/min}$ ).

Figure 2 shows a correlation between the volumetrically determined  $\text{HNO}_3$  standard concentration and the calculated concentration using the procedure described in Sect. 2.1. The error bars represent the systematic variation in measurements. The value of the slope of Fig. 2 corresponds to the calibration factor used to compensate the difference between the true values and the adapted values of the calculation parameters, i.e., the ion-molecule reaction rate constant, reduced ionic mobility, quadrupole transmission efficiency, and etc. For five independent calibrations at  $25^\circ\text{C}$ , a calibration factor of  $2.2 \pm 0.2$  is obtained.

$\text{N}_2\text{O}_5$  calibration is conducted with laboratory synthesized samples (Huey et al., 1995).  $\text{N}_2\text{O}_5$  is formed through two sequential reactions (Reactions 3 and 4).  $\text{O}_3$  and  $\text{NO}_2$  are mixed in a sealed glass reactor and the produced  $\text{N}_2\text{O}_5$  is collected in a cryotrap ( $-78.5^\circ\text{C}$ ) as white crystal. The first batch of  $\text{N}_2\text{O}_5$  is discarded to remove the water residue inside the cryotrap. During calibration, pure  $\text{N}_2\text{O}_5$  is kept in an octanol/dry ice bath ( $-57^\circ\text{C}$ ). A small amount of dry  $\text{N}_2$  flows through the container and carries  $\text{N}_2\text{O}_5$  vapor into a 10-cm long absorption cell inside a UV/VIS spectrometer (Perkin Elmer), where the absolute concentration of  $\text{N}_2\text{O}_5$  is measured by its absorption at  $215 \text{ nm}$  ( $\sigma = 2.95 \times 10^{-18} \text{ cm}^2 \text{ molecule}^{-1}$ , JPL 2006). The concentrated  $\text{N}_2\text{O}_5$  flow is diluted into a  $140 \text{ slpm}$  flow and analyzed by the ID-CIMS. Because  $\text{N}_2\text{O}_5$  is in thermodynamic equilibrium with  $\text{NO}_2$  and  $\text{NO}_3$  (Reaction 4) and  $\text{NO}_3$  can also be

[Title Page](#)[Abstract](#)[Introduction](#)[Conclusions](#)[References](#)[Tables](#)[Figures](#)[◀](#)[▶](#)[◀](#)[▶](#)[Back](#)[Close](#)[Full Screen / Esc](#)[Printer-friendly Version](#)[Interactive Discussion](#)

detected, we estimate its potential interference and find that only less than 6% of initial  $\text{N}_2\text{O}_5$  decomposes into  $\text{NO}_3$  at room temperature. Figure 3 shows the plots of the  $\text{N}_2\text{O}_5$  concentrations measured by ID-CIMS against the concentrations determined from UV absorption. The slope in Fig. 3 represents the calibration factor.

During the field measurements,  $\text{HNO}_3$  background checks are performed once a few hours by directing the ambient air flow through a two-inch OD nylon filter.  $\text{N}_2\text{O}_5$  background signal is checked by passing the ambient air mixed with several hundreds of ppb  $\text{NO}$  through a 12-in-long heated metal tubing. Detection limits of  $\text{HNO}_3$  and  $\text{N}_2\text{O}_5$  for 10 s integration time are estimated about 100 ppt and 20 ppt, respectively.

## 2.4 Field setup and characterization of the inlet

The ID-CIMS instrument was deployed at the T0 supersite, located at the Instituto Mexicano del Petróleo (IMP) near the center of the Mexico City Basin ( $19^\circ 29.400' \text{ N}$ ,  $99^\circ 08.911' \text{ W}$ ). The ID-CIMS was housed inside an air-conditioned hut on the roof of Bldg. 32, which was about 30 m above the ground and among a cluster of buildings with the similar height. A 2.20 cm ID PFA tubing was used as the inlet, which had been proved to be the best inlet material (Neuman et al., 1999). In order to minimize the surface effect, ambient air was sampled from two feet above the hut ceiling, and the inlet length was about 12 feet to bring the air sample into the ID-CIMS, located a few inches away from the sampling window. During most times of the field campaign, the weather was dry and relatively cold. Because  $\text{HNO}_3$  gas-aerosol partitioning was sensitive to temperature variations, no heating was applied to the  $\text{HNO}_3$  inlet. Instead, the sampling flow rate was kept at 200 slpm to minimize the sampling residence time (0.42 s) and the entire inlet was kept under the ambient conditions.

In order to characterize the inlet performance, several tests were conducted by exposing the inlet to  $\text{HNO}_3$  (performed at 760 torr,  $25^\circ\text{C}$ ,  $\text{RH}=50\%$ ). The front of the inlet was exposed to a solution of 68 wt%  $\text{HNO}_3$  for less than one second and the ID-CIMS was set to collect data at 0.4 Hz. As shown in Fig. 4, a spike of about 40 ppb  $\text{HNO}_3$  was detected by the ID-CIMS within 3 s and the  $\text{HNO}_3$  signal immediately decreased

[Title Page](#)[Abstract](#)[Introduction](#)[Conclusions](#)[References](#)[Tables](#)[Figures](#)[◀](#)[▶](#)[◀](#)[▶](#)[Back](#)[Close](#)[Full Screen / Esc](#)[Printer-friendly Version](#)[Interactive Discussion](#)

by about 80% after 9 s. The decay in the  $\text{HNO}_3$  signal was well-fixed by an exponential decay function ( $[\text{HNO}_3]=2.4+97.5 \exp(-0.237t)$ ), showing that the inlet had little memory effect. The influence between adjacent data points was less than 20% relative to each other, if data were collected within every 9 s.

The inlet for  $\text{N}_2\text{O}_5$  measurements was also made from 2.2 cm ID Teflon tubing except that its length was only 2 ft to minimize surface loss.

An Aerodyne aerosol mass spectrometer (AMS) was used to measure the chemical composition of non-refractory aerosols from 35 nm to 1.5  $\mu\text{m}$  in size. This version of AMS was equipped with a high-resolution time-of-flight mass analyzer and was capable of analyzing organic species and most nitrate and sulfate compounds of different elemental compositions at the same nominal  $m/z$ . More details about the AMS were described by DeCarlo et al. (2006).

An ICMS was set up at T0 to measure both gas and aerosol phase acids. Air was aspirated through a wet effluent diffusion denuder (WEDD) at 2 L/min to sample the gas phase acids. Water was continuously pumped through the denuder at a flow rate of 2 mL/min at counter flow to the air. The air to the aerosol collector (AC) first passed at 4 L/min through an activated charcoal denuder to remove the gas phase. The air stream was mixed with heated water vapor (100°C and a flow rate of 0.6 ml/min), which condensed on the aerosol particles. These droplets impacted on a cooled maze (Fisseha et al., 2006). The gas phase as well as the particle phase extracts were collected on a concentrator column (TAC-LP1, Dionex) and analyzed alternately using ion chromatography (conductivity detector) with a mass spectrometer in a quasi-continuous mode. The mass spectrometer (MSQ from Dionex) used electro-spray ionization and had a single quadrupole mass detector.

$\text{NO}_x$  and  $\text{O}_3$  data used in this work were measured by commercial instruments (Thermo Scientific). Both instruments were regularly calibrated during the campaign. The detection limits were 0.2 ppb for each species and the data were collected at 1-min interval.

**Nitric acid during  
MCMA 2006**

R. Zhang et al.

Title Page

Abstract

Introduction

Conclusions

References

Tables

Figures

I◀

▶I

◀

▶

Back

Close

Full Screen / Esc

Printer-friendly Version

Interactive Discussion



### 3 Results and discussion

#### 3.1 HNO<sub>3</sub> Measurements

The measurements of HNO<sub>3</sub> and N<sub>2</sub>O<sub>5</sub> were conducted from 7 March to 30 March during the MCMA 2006. Due to a power supply failure, measurements from 13 March to 17 March were not available. The ID-CIMS was typically setup to measure HNO<sub>3</sub> during the daytime and after sunset it was switched to the N<sub>2</sub>O<sub>5</sub> measurement. All data was collected at 0.1 Hz and presented in CST.

Figure 5 shows a diurnal profile of HNO<sub>3</sub> observed on 22 March, a sunny and hazy day. Due to its photochemical production nature, HNO<sub>3</sub> started to slowly accumulate right after sunrise. From 08:30 a.m. to 10:00 a.m., about 200 ppt HNO<sub>3</sub> was observed and no significant increase occurred before 11:00 a.m. After a steadily increase, HNO<sub>3</sub> reached near 3 ppb at 02:00 p.m., when the photochemical activity reached the maximum. From 02:00 p.m. to 04:00 p.m., HNO<sub>3</sub> reached a peak, and started to decrease sharply after 04:00 p.m. Within one and half hours, only about 400 ppt was observed. HNO<sub>3</sub> did not totally disappear even after it was completely dark, indicating that there were likely other HNO<sub>3</sub> sources sustaining its present. However, when the ID-CIMS was switched into the N<sub>2</sub>O<sub>5</sub> mode, no detectable N<sub>2</sub>O<sub>5</sub> was observed.

Figure 6 depicts another HNO<sub>3</sub> diurnal profile observed on 23 March, which was relatively cleaner and windier than the previous day. Before 09:00 a.m., HNO<sub>3</sub> was close the instrument detection limit. Shortly after, HNO<sub>3</sub> increased steadily to about 1 ppb at 11:30 a.m. and, then, started to decrease to 600 ppt at 01:00 p.m., when HNO<sub>3</sub> production was supposedly to be maximized. Around 02:45 p.m., HNO<sub>3</sub> started to increase again and reached a daily maximum 1.5 ppb. HNO<sub>3</sub> decreased steadily to 400 ppt at 04:00 p.m. Similar to the previous day observation, near 300 ppt HNO<sub>3</sub> was still observable at about 06:30 p.m. Also, when the ID-CIMS was switched into the N<sub>2</sub>O<sub>5</sub> mode, no N<sub>2</sub>O<sub>5</sub> was observable. Note that 22 March and 23 represented the typical polluted and clean conditions encountered during the field campaign, respectively.

Figure 7 shows the HNO<sub>3</sub> diurnal profile averaged over the entire campaign. Typ-

Title Page

Abstract

Introduction

Conclusions

References

Tables

Figures

◀

▶

◀

▶

Back

Close

Full Screen / Esc

Printer-friendly Version

Interactive Discussion



**Nitric acid during  
MCMA 2006**

R. Zhang et al.

ically, no significant  $\text{HNO}_3$  was observed before 08:00 a.m., and  $\text{HNO}_3$  started to accumulate after 09:00 a.m. and reached daily high,  $1 \pm 0.65$  ppb, between 02:00 to 03:00 p.m. After 04:00 p.m.,  $\text{HNO}_3$  decreased rapidly to less than 0.4 ppb at 06:00 p.m. and gradually approached 200 ppt, before the ID-CIMS was switched to  $\text{N}_2\text{O}_5$  measurements. The occurrence of the  $\text{HNO}_3$  daily peak was consistent with its photochemical production mechanism, however the magnitude of the  $\text{HNO}_3$  peak was lower than that expected given the overwhelming  $\text{NO}_x$  emission inventory in the MCMA and the strong tropical solar radiation. Another interesting observation was that several hundred ppt  $\text{HNO}_3$  was still detected several hours after sunset. Since no significant  $\text{N}_2\text{O}_5$  was present, the nighttime production of  $\text{HNO}_3$  from the hydrolysis of  $\text{N}_2\text{O}_5$  (through Reactions 2 to 5) could not proceed.

It is evident that the gas-phase chemistry alone could not explain the observed slow rise in the  $\text{HNO}_3$  diurnal profiles after sunrise and the residual  $\text{HNO}_3$  amount after sunset during MCMA 2006. Heterogeneous processing of  $\text{HNO}_3$  in the particle phase needs to be accounted for to explain the  $\text{HNO}_3$  measurements (Zhang et al., 1993). It has been suggested that the heterogeneous reaction between  $\text{HNO}_3$  and  $\text{NH}_3$  in the particle-phase represents an important process to modulate the gaseous  $\text{HNO}_3$  concentration (Seinfeld and Pandis, 1998),



Depending on the ambient relative humidity (RH), ammonium nitrate formed in Reaction 18 can exist as a solid or an aqueous solution of  $\text{NH}_4^+$  and  $\text{NO}_3^-$ . The equilibrium constant,  $K_p$ , is dependent on the temperature,

$$\ln K_p = 84.6 - (24220/T) - 6.1 \times \ln(T/298) \quad (19)$$

For the measurements relevant to MCMA 2006, the RH was fairly low (<41% averaged over the campaign period). The dry environment at the MCMA prevented  $\text{NH}_4\text{NO}_3$  from deliquescence and  $\text{NH}_4\text{NO}_3$  was expected in a solid state. High ammonia ( $\text{NH}_3$ ) concentration (>35 ppb in the early morning) was reported during the MCMA 2003

[Title Page](#)[Abstract](#)[Introduction](#)[Conclusions](#)[References](#)[Tables](#)[Figures](#)[I◀](#)[▶I](#)[◀](#)[▶](#)[Back](#)[Close](#)[Full Screen / Esc](#)[Printer-friendly Version](#)[Interactive Discussion](#)

campaign (Moya et al., 2004). Although no direct measurements of  $\text{NH}_3$  was available at T0 during MCMA 2006, its concentration is expected to be high, given that both population and traffic activity inside the MCMA maintained an increasing trend since 2003.

5 Figure 8 shows a comparison between gaseous  $\text{HNO}_3$  and aerosol nitrate ( $\text{NO}_3^-$ ) mass concentration measured by an Aerodyne aerosol mass spectrometer (AMS) on 22 and 23 March. The calculated equilibrium constant ( $K_p$ ) of Reaction 18 is also plotted in Fig. 8, which is a function of ambient temperature. There are several prominent features in Fig. 8. The aerosol nitrate  $\text{NO}_3^-$  started to increase right after sunrise and reached a maximum in the early morning. The aerosol nitrate peak occurred several hours earlier than that of the gaseous  $\text{HNO}_3$  concentration. The aerosol nitrate dropped sharply after the morning peak and remained low throughout the afternoon and night hours. During each day, the measured  $\text{HNO}_3$  concentration and the calculated  $K_p$  were anti-correlated with  $\text{NO}_3^-$ . On the other hand, there appeared to have a good correlation between the measured  $\text{HNO}_3$  concentration and calculated  $K_p$ : both slowly increased at the morning hours and their peaks coincided. Hence, the slow rise in the measured  $\text{HNO}_3$  concentration is likely explained by gas/aerosol partitioning.  $\text{HNO}_3$  photochemically produced from Reaction 1 was scavenged from the gas phase by the particle-phase reaction with  $\text{NH}_3$  to form aerosol nitrate, when ambient temperature was low and aerosol nitrate was favorable ( $K_p < 6$ ). The gas/aerosol partitioning hence accounts for the delayed rise and daily maximum of measured  $\text{HNO}_3$  compared to those of measured aerosol nitrate. As the temperature rose during the course of the day, the equilibrium favored gaseous  $\text{HNO}_3$ .  $\text{HNO}_3$  was released back to gas-phase from the evaporation of aerosol nitrate, even when its photochemical production decreased. After sunset, the  $\text{HNO}_3$  photochemical production ceased, as reflected in the sharp decrease in measured  $\text{HNO}_3$ , while a few hundreds of ppt  $\text{HNO}_3$  were still measured. Since detectable  $\text{NO}_3^-$  was present and no detectable  $\text{N}_2\text{O}_5$  was observed, the lingering nighttime  $\text{HNO}_3$  likely originated from the residue ammonium nitrate aerosol, instead from the hydrolysis of  $\text{N}_2\text{O}_5$ . Figure 8 also shows that on a daily basis higher

**Nitric acid during  
MCMA 2006**

R. Zhang et al.

[Title Page](#)[Abstract](#)[Introduction](#)[Conclusions](#)[References](#)[Tables](#)[Figures](#)[◀](#)[▶](#)[◀](#)[▶](#)[Back](#)[Close](#)[Full Screen / Esc](#)[Printer-friendly Version](#)[Interactive Discussion](#)

**Nitric acid during  
MCMA 2006**

R. Zhang et al.

aerosol nitrate corresponded to a higher  $\text{HNO}_3$  peak, when the difference in  $K_p$  was insignificant. This explains the difference in the measurements of  $\text{NO}_3^-$  and  $\text{HNO}_3$  between 22 and 23 March 2006. Therefore, we concluded that during MCMA 2006 at T0 gas/particle partitioning played a key role to account for the measurements in gaseous  $\text{HNO}_3$  and aerosol nitrate.

The magnitude and diurnal cycle of aerosol nitrate during the MCMA 2003 was reported by Salcedo et al. (2006). In the morning, particulate nitrate increased and was consistent with the production of nitric acid. However, after 11:00 a.m. aerosol nitrate decreased while  $\text{HNO}_3$  production continued. This observation was explained by the increase in the PBL height and temperature and the decrease in the RH as the day progressed. Also, it has been suggested that gas-particle partitioning plays a dominant role in the fate of aerosol nitrate over larger spatial scales (DeCarlo et al., 2007).

### 3.2 $\text{N}_2\text{O}_5$ measurements

The ID-CIMS instrument was typically switched to conduct  $\text{N}_2\text{O}_5$  measurements after sunset during the 2006 MCMA campaign. During most times of the campaign, nighttime  $\text{N}_2\text{O}_5$  was below the detection limit of the instrument. Because NO concentration frequently exceeded 100 ppb after 07:00 p.m. and  $\text{O}_3$  was quickly depleted by the freshly emitted NO, Reactions 3 and 4 were inhibited at the surface level. Therefore,  $\text{NO}_3$  and  $\text{N}_2\text{O}_5$  did not play a major role during the nighttime chemistry on the surface. It was still likely that some  $\text{HNO}_3$  might be formed above the planetary boundary layer (PBL) where the  $\text{N}_2\text{O}_5$  chemistry was still occurring at night and mixed downward (Stutz et al., 2004). However, as an exception, two  $\text{N}_2\text{O}_5$  peaks were observed in the late afternoon and early evening on March 26 (Fig. 9). There was a scattered shower started in the early afternoon and no  $\text{HNO}_3$  was observed thereafter. At 04:00 p.m., the rain stopped and the sky remained cloudy, and  $\text{O}_3$  and  $\text{NO}_2$  were about 60 ppb and 20 ppb, respectively. Meanwhile, the NO concentration was less than 2 ppb. The ID-CIMS was switched to the  $\text{N}_2\text{O}_5$  mode at 04:20 p.m. and continued the measurement until 09:40 p.m., when NO and  $\text{NO}_2$  were about 40 ppb and 60 ppb but  $\text{O}_3$  was

[Title Page](#)[Abstract](#)[Introduction](#)[Conclusions](#)[References](#)[Tables](#)[Figures](#)[I◀](#)[▶I](#)[◀](#)[▶](#)[Back](#)[Close](#)[Full Screen / Esc](#)[Printer-friendly Version](#)[Interactive Discussion](#)

only 3 ppb. Background checks were performed at the beginning and the end of the measurement. Two  $\text{N}_2\text{O}_5$  peaks near 40 ppt were observed around 05:00 p.m. and 08:00 p.m., when both  $\text{NO}_2$  and  $\text{O}_3$  were still substantial, but no fresh NO emission was present. From 05:45 p.m. to 07:20 p.m., the T0 site was hit by another intermittent shower, and no  $\text{N}_2\text{O}_5$  was observed and the  $\text{NO}_x$  and  $\text{O}_3$  instruments were off-line for calibrations. After 07:30 p.m.,  $\text{O}_3$  was anti-correlated with  $\text{NO}_2$  due to the NO titration. About 08:50 p.m., NO started to increase significantly and nearly all  $\text{O}_3$  was depleted, as  $\text{N}_2\text{O}_5$  disappeared. Although the ID-CIMS could also response to  $\text{NO}_3$  radical as  $\text{NO}_3^-$  at the same  $m/e=62$  peak,  $\text{NO}_3$  radical was estimated to be less than 4% of the  $\text{N}_2\text{O}_5$  signal assuming that Reaction 4 was under thermodynamic equilibrium and using the observed  $\text{NO}_2$  and  $\text{O}_3$  concentrations.

### 3.3 Inter-comparison with ICMS

An ICMS instrument was set up side-by-side with the ID-CIMS during the MCMA 2006 field campaign. The ICMS utilized a denuder to selectively collect gas phase  $\text{HNO}_3$  into aqueous solutions, which were then analyzed by an electrospray mass spectrometer. The ICMS generated one data point about every two hours, thus its time series could not match with the temporal resolution of about 10 s from the ID-CIMS measurements. We compared the results between the two instruments for periods when both instruments were collecting data and the ID-CIMS data were averaged to represent the data during a similar period. The results were plotted in Fig. 10. A good correlation in performance was found ( $R^2=0.75$ ) between the two techniques. We also performed a  $t$ -test for these two set of data and a  $P$  value of 0.68 further proved that statistically these two techniques reported the same results. The ID-CIMS data set was about 17% lower than the ICMS data set, and the intersection was well below the detection limit of either instrument.

Title Page

Abstract

Introduction

Conclusions

References

Tables

Figures

◀

▶

◀

▶

Back

Close

Full Screen / Esc

Printer-friendly Version

Interactive Discussion



## 4 Conclusions

We deployed an ID-CIMS during the MCMA 2006 campaign to measure  $\text{HNO}_3$  and  $\text{N}_2\text{O}_5$  at the T0 site. The objective of this work is to characterize the  $\text{NO}_x$  chemistry and its budget in the MCMA. Diurnally,  $\text{HNO}_3$  was less than 200 parts per trillion (ppt) during the night and in the early morning, increased steadily from around 09:00 a.m. CST, reached a peak value of 0.5 to 3 parts per billion (ppb) in the early afternoon, and declined sharply to less than half of the peak value near 05:00 p.m. CST. The  $\text{HNO}_3$  mixing ratio was found to anti-correlate with aerosol nitrate, suggesting that the gaseous  $\text{HNO}_3$  concentration was regulated by the gas-particle partitioning process. Inter-comparison between the ID-CIMS and the ICMS showed a good agreement ( $R^2=0.75$ ) in  $\text{HNO}_3$  measurements. During most times of the MCMA 2006 campaign,  $\text{N}_2\text{O}_5$  was below the detection limit of the ID-CIMS due to high  $\text{NO}$  mixing ratio at the surface, with one exception of transient  $\text{N}_2\text{O}_5$  peaks of 40 ppt were encountered on 26 March under cloudy conditions. The results reveal that during the MCMA 2006 campaign  $\text{HNO}_3$  was primarily produced through the photochemical process and  $\text{HNO}_3$  diurnal profile was largely controlled by the gas/particle partitioning process.

*Acknowledgements.* This research was funded by the Center for Atmospheric Chemistry and Environment at the Texas A & M University. The authors were grateful to N. A. Marley and J. S. Gaffney for providing the temperature and RH data.

## References

- Anlauf, K. G., Mactavish, D. C., Wiebe, H. A., Schiff, H. I., and Mackay, G. I.: Measurement of atmospheric nitric-acid by the filter method and comparisons with the tunable diode-laser and other methods, *Atmos. Environ.*, 22, 1579–1586, 1988.
- Brown, S. S., Stark, H., Ciciora, S. J., and Ravishankara, A. R.: In-situ measurement of atmospheric  $\text{NO}_3$  and  $\text{N}_2\text{O}_5$  via cavity ring-down spectroscopy, *Geophys. Res. Lett.*, 28, 3227–3230, 2001.

Title Page

Abstract

Introduction

Conclusions

References

Tables

Figures

◀

▶

◀

▶

Back

Close

Full Screen / Esc

Printer-friendly Version

Interactive Discussion



**Nitric acid during  
MCMA 2006**

R. Zhang et al.

[Title Page](#)[Abstract](#)[Introduction](#)[Conclusions](#)[References](#)[Tables](#)[Figures](#)[◀](#)[▶](#)[◀](#)[▶](#)[Back](#)[Close](#)[Full Screen / Esc](#)[Printer-friendly Version](#)[Interactive Discussion](#)

Brown, S. S., Stark, H., Ciciora, S. J., McLaughlin, R. J., and Ravishankara, A. R.: Simultaneous in situ detection of atmospheric  $\text{NO}_3$  and  $\text{N}_2\text{O}_5$  via cavity ring-down spectroscopy, *Rev. Sci. Instrum.*, 73, 3291–3301, 2002.

Brown, S. S., Ryerson, T. B., Wollny, A. G., Brock, C. A., Peltier, R., Sullivan, A. P., Weber, R. J., Dube, W. P., Trainer, M., Meagher, J. F., Fehsenfeld, F. C., and Ravishankara, A. R.: Variability in nocturnal nitrogen oxide processing and its role in regional air quality, *Science*, 311, 67–70, 2006.

DeCarlo, P. F., Kimmel, J. R., Trimborn, A., Northway, M. J., Jayne, J. T., Aiken, A. C., Gonin, M., Fuhrer, K., Horvath, T., Docherty, K. S., Worsnop, D. R., and Jimenez, J. L.: Field-deployable, high-resolution, time-of-flight aerosol mass spectrometer, *Anal. Chem.*, 78, 8281–8289, 2006.

DeCarlo, P. F., Dunlea, E. J., Kimmel, J. R., Aiken, A. C., Sueper, D., Crouse, J., Wennberg, P. O., Emmons, L., Shinozuka, Y., Clarke, A., Zhou, J., Tomlinson, J., Collins, D. R., Knapp, D., Weinheimer, A. J., Montzka, D. D., Campos, T., and Jimenez, J. L.: Fast airborne aerosol size and chemistry measurements with the high resolution aerosol mass spectrometer during the milagro campaign, *Atmos. Chem. Phys. Discuss.*, 7, 18269–18317, 2007.

Fisseha, R., Dommen, J., Gaeggeler, K., Weingartner, E., Samburova, V., Kalberer, M., and Baltensperger, U.: Online gas and aerosol measurement of water soluble carboxylic acids in zurich, *J. Geophys. Res.*, 111, D12316, doi:10.1029/2005JD006782, 2006.

Finlayson-Pitts, B. J. and Pitts, J. N.: *Chemistry of the upper and lower atmosphere : Theory, experiments and applications*, Academic Press, San Diego, Calif., xxii, 969 pp., 1999.

Fortner, E. C., Zhao, J., and Zhang, R. Y.: Development of ion drift-chemical ionization mass spectrometry, *Anal. Chem.*, 76, 5436–5440, 2004.

Furutani, H. and Akimoto, H.: Development and characterization of a fast measurement system for gas-phase nitric acid with a chemical ionization mass spectrometer in the marine boundary layer, *J. Geophys. Res.-Atmos.*, 107, 4016, doi:10.1029/2000JD000269, 2002.

Hering, S. V., Lawson, D. R., Allegrini, I., Febo, A., Perrino, C., Possanzini, M., Sickles, J. E., Anlauf, K. G., Wiebe, A., Appel, B. R., John, W., Ondo, J., Wall, S., Braman, R. S., Sutton, R., Cass, G. R., Solomon, P. A., Eatough, D. J., Eatough, N. L., Ellis, E. C., Grosjean, D., Hicks, B. B., Womack, J. D., Horrocks, J., Knapp, K. T., Ellestad, T. G., Paur, R. J., Mitchell, W. J., Pleasant, M., Peake, E., Maclean, A., Pierson, W. R., Brachaczek, W., Schiff, H. I., Mackay, G. I., Spicer, C. W., Stedman, D. H., Winer, A. M., Biermann, H. W., and Tuazon, E. C.: The nitric-acid shootout – field comparison of measurement methods, *Atmos. Environ.*,

22, 1519–1539, 1988.

Huey, L. G., Hanson, D. R., and Howard, C. J.: Reactions of  $\text{SF}_6^-$  and  $\text{I}^-$  with atmospheric trace gases, *J. Phys. Chem.*, 99, 5001–5008, 1995.

Huey, L. G. and Lovejoy, E. R.: Reactions of  $\text{SiF}_5^-$  with atmospheric trace gases: Ion chemistry for chemical ionization detection of  $\text{HNO}_3$  in the troposphere, *Int. J. Mass. Spectrom.*, 155, 133–140, 1996.

Huey, L. G., Dunlea, E. J., Lovejoy, E. R., Hanson, D. R., Norton, R. B., Fehsenfeld, F. C., and Howard, C. J.: Fast time response measurements of  $\text{HNO}_3$  in air with a chemical ionization mass spectrometer, *J. Geophys. Res.-Atmos.*, 103, 3355–3360, 1998.

Huey, L. G., Tanner, D. J., Slusher, D. L., Dibb, J. E., Arimoto, R., Chen, G., Davis, D., Buhr, M. P., Nowak, J. B., Mauldin, R. L., Eisele, F. L., and Kosciuch, E.: CIMS measurements of  $\text{HNO}_3$  and  $\text{SO}_2$  at the south pole during ISCAT 2000, *Atmos. Environ.*, 38, 5411–5421, 2004.

Huey, L. G.: Measurement of trace atmospheric species by chemical ionization mass spectrometry: Speciation of reactive nitrogen and future directions, *Mass Spectrom. Rev.*, 26, 166–184, 2007.

JPL: Chemical Kinetics and Photochemical Data for Use in Atmospheric Studies Evaluation Number 15, National Aeronautics and Space Administration, Jet Propulsion Laboratory, California Institute of Technology, Pasadena, Calif., 5–77, 2006.

Lei, W., de Foy, B., Zavala, M., Volkamer, R., and Molina, L. T.: Characterizing ozone production in the Mexico City metropolitan area: A case study using a chemical transport model, *Atmos. Chem. Phys.*, 7, 1347–1366, 2007, <http://www.atmos-chem-phys.net/7/1347/2007/>.

Lei, W. F., Derecskei-Kovacs, A., and Zhang, R. Y.: Ab initio study of oh addition reaction to isoprene, *J. Chem. Phys.*, 113, 5354–5360, 2000.

Lei, W. F. and Zhang, R. Y.: Theoretical study of hydroxylisoprene alkoxy radicals and their decomposition pathways, *J. Phys. Chem. A*, 105, 3808–3815, 2001.

Lei, W. F., Zhang, R. Y., Tie, X. X., and Hess, P.: Chemical characterization of ozone formation in the Houston-Galveston area: A chemical transport model study, *J. Geophys. Res.-Atmos.*, 109, D12301, doi:10.1029/2003JD004219, 2004.

Mason, E. A. and McDaniel, E. W.: Transport properties of ions in gases, Wiley, New York, xvi, 560 pp., 1988.

Molina, L. T., Molina, M. J., and Alliance for Global Sustainability: Air quality in the Mexico megacity: An integrated assessment, Alliance for global sustainability bookseries; 2, Kluwer

**Nitric acid during  
MCMA 2006**

R. Zhang et al.

Title Page

Abstract

Introduction

Conclusions

References

Tables

Figures

◀

▶

◀

▶

Back

Close

Full Screen / Esc

Printer-friendly Version

Interactive Discussion



**Nitric acid during  
MCMA 2006**

R. Zhang et al.

Title Page

Abstract

Introduction

Conclusions

References

Tables

Figures

◀

▶

◀

▶

Back

Close

Full Screen / Esc

Printer-friendly Version

Interactive Discussion



Academic Publishers, Dordrecht; Boston, xxi, 384 pp., 2002.

Molina, L. T., Kolb, C. E., de Foy, B., Lamb, B. K., Brune, W. H., Jimenez, J. L., Ramos-Villegas, R., Sarmiento, J., Paramo-Figueroa, V. H., Cardenas, B., Gutierrez-Avedoy, V., and Molina, M. J.: Air quality in north America's most populous city—overview of the MCMA-2003 campaign, *Atmos. Chem. Phys.*, 7, 2447–2473, 2007, <http://www.atmos-chem-phys.net/7/2447/2007/>.

Moya, M., Grutter, M., and Baez, A.: Diurnal variability of size-differentiated inorganic aerosols and their gas-phase precursors during January and February of 2003 near downtown Mexico City, *Atmos. Environ.*, 38, 5651–5661, 2004.

Neuman, J. A., Huey, L. G., Ryerson, T. B., and Fahey, D. W.: Study of inlet materials for sampling atmospheric nitric acid, *Environ. Sci. Technol.*, 33, 1133–1136, 1999.

Perrino, C., Desantis, F., and Febo, A.: Criteria for the choice of a denuder sampling technique devoted to the measurement of atmospheric nitrous and nitric-acids, *Atmos. Environ. A-Gen.*, 24, 617–626, 1990.

Ramazan, K. A., Wingen, L. M., Miller, Y., Chaban, G. M., Gerber, R. B., Xantheas, S. S., and Finlayson-Pitts, B. J.: New experimental and theoretical approach to the heterogeneous hydrolysis of  $\text{NO}_2$ : Key role of molecular nitric acid and its complexes, *J. Phys. Chem. A*, 110, 6886–6897, doi:10.1021/Jp056426n, 2006.

Saliba, N. A., Yang, H., and Finlayson-Pitts, B. J.: Reaction of gaseous nitric oxide with nitric acid on silica surfaces in the presence of water at room temperature, *J. Phys. Chem. A*, 105, 10 339–10 346, doi:10.1021/Jp012330r, 2001.

Salcedo, D., Onasch, T. B., Dzepina, K., Canagaratna, M. R., Zhang, Q., Huffman, J. A., DeCarlo, P. F., Jayne, J. T., Mortimer, P., Worsnop, D. R., Kolb, C. E., Johnson, K. S., Zuberi, B., Marr, L. C., Volkamer, R., Molina, L. T., Molina, M. J., Cardenas, B., Bernabe, R. M., Marquez, C., Gaffney, J. S., Marley, N. A., Laskin, A., Shutthanandan, V., Xie, Y., Brune, W., Leshner, R., Shirley, T., and Jimenez, J. L.: Characterization of ambient aerosols in Mexico city during the mcma-2003 campaign with aerosol mass spectrometry: Results from the cenica supersite, *Atmos. Chem. Phys.*, 6, 925–946, 2006, <http://www.atmos-chem-phys.net/6/925/2006/>.

Seinfeld J. H. and Pandis, S. N.: From air pollution to climate change, Wiley, New York, xxvii, *Atmos. Chem. Phys.*, 1326 pp., 1998.

Sillman, S.: The relation between ozone,  $\text{NO}_x$  and hydrocarbons in urban and polluted rural environments, *Atmos. Environ.*, 33, 1821–1845, 1999.

**Nitric acid during  
MCMA 2006**

R. Zhang et al.

[Title Page](#)[Abstract](#)[Introduction](#)[Conclusions](#)[References](#)[Tables](#)[Figures](#)[◀](#)[▶](#)[◀](#)[▶](#)[Back](#)[Close](#)[Full Screen / Esc](#)[Printer-friendly Version](#)[Interactive Discussion](#)

- Simon, P. K. and Dasgupta, P. K.: Continuous automated measurement of gaseous nitrous and nitric-acids and particulate nitrite and nitrate, *Environ. Sci. Technol.*, 29, 1534–1541, 1995.
- Slusher, D. L., Huey, L. G., Tanner, D. J., Flocke, F. M., and Roberts, J. M.: A thermal dissociation-chemical ionization mass spectrometry (td-cims) technique for the simultaneous measurement of peroxyacyl nitrates and dinitrogen pentoxide, *J. Geophys. Res.-Atmos.*, 109, D19315, 2004.
- Stutz, J., Alicke, B., Ackermann, R., Geyer, A., White, A., and Williams, E.: Vertical profiles of  $\text{NO}_3$ ,  $\text{N}_2\text{O}_5$ ,  $\text{O}_3$ , and  $\text{NO}_x$  in the nocturnal boundary layer: 1. Observations during the texas air quality study 2000, *J. Geophys. Res.*, 109, D12306, doi:10.1029/2003JD004209, 2004.
- Suh, I., Lei, W. F., and Zhang, R. Y.: Experimental and theoretical studies of isoprene reaction with  $\text{NO}_3$ , *J. Phys. Chem. A*, 105, 6471–6478, 2001.
- Talbot, R. W., Vijgen, A. S., and Harriss, R. C.: Measuring tropospheric hno3 - problems and prospects for nylon filter and mist chamber techniques, *J. Geophys. Res.-Atmos.*, 95, 7553–7561, 1990.
- Tie, X. X., Madronich, S., Li, G. H., Ying, Z. M., Zhang, R. Y., Garcia, A. R., Lee-Taylor, J., and Liu, Y. B.: Characterizations of chemical oxidants in mexico city: A regional chemical dynamical model (wrf-chem) study, *Atmos. Environ.*, 41, 1989–2008, 2007.
- Viehland, L. A., Mason, E. A., Morrison, W. F., and Flannery, M. R.: Tables of transport collision integrals for (n, 6, 4) ion-neutral potentials, *Atom. Data Nucl. Data*, 16, 495–514, 1975.
- Zhang, R., Wooldridge, P. J., and Molina, M. J.: Vapor pressure measurements for the  $\text{H}_2\text{SO}_4/\text{HNO}_3/\text{H}_2\text{O}$  and  $\text{H}_2\text{SO}_4/\text{HCl}/\text{H}_2\text{O}$  systems: Incorporation of stratospheric acids into background sulfate aerosols, *J. Phys. Chem.*, 97, 8541–8548, 1993.
- Zhang, R. Y., Leu, M. T., and Keyser, L. F.: Hydrolysis of  $\text{N}_2\text{O}_5$  and  $\text{ClONO}_2$  on the  $\text{H}_2\text{SO}_4/\text{HNO}_3/\text{H}_2\text{O}$  ternary solutions under stratospheric conditions, *Geophys. Res. Lett.*, 22, 1493–1496, 1995.
- Zhang, R. Y., Lei, W. F., Tie, X. X., and Hess, P.: Industrial emissions cause extreme urban ozone diurnal variability, *P. Natl. Acad. Sci. USA*, 101, 6346–6350, 2004a.
- Zhang, R. Y., Suh, I., Zhao, J., Zhang, D., Fortner, E. C., Tie, X. X., Molina, L. T., and Molina, M. J.: Atmospheric new particle formation enhanced by organic acids, *Science*, 304, 1487–1490, 2004b.
- Zhao, J. and Zhang, R. Y.: Proton transfer reaction rate constants between hydronium ion ( $\text{H}_3\text{O}^{(+)}$ ) and volatile organic compounds, *Atmos. Environ.*, 38, 2177–2185, 2004.

**Nitric acid during  
MCMA 2006**

R. Zhang et al.

**Table 1.** Ion-neutral potentials of  $\text{SiF}_5^-/\text{N}_2$  and  $\text{I}^-/\text{N}_2$  systems based on ab initio calculations.

	$\text{SiF}_5^-/\text{N}_2$	$\text{I}^-/\text{N}_2$
$\varepsilon$ (eV)	0.050	0.057
$r_m$ (Å)	4.82	4.06
$B$ ( $\text{eV}\cdot\text{Å}^{12}$ )	$8.62\times 10^6$	$5.29\times 10^5$
$C_6$ ( $\text{eV}\cdot\text{Å}^6$ )	824.96	220.38
$C_4$ ( $\text{eV}\cdot\text{Å}^4$ )	20.98	8.39
$\bar{\Omega}$ ( $10^{-16}\text{cm}^2$ )	73.16	51.83

[Title Page](#)
[Abstract](#)
[Introduction](#)
[Conclusions](#)
[References](#)
[Tables](#)
[Figures](#)
[I◀](#)
[▶I](#)
[◀](#)
[▶](#)
[Back](#)
[Close](#)
[Full Screen / Esc](#)
[Printer-friendly Version](#)
[Interactive Discussion](#)


Nitric acid during  
MCMA 2006

R. Zhang et al.

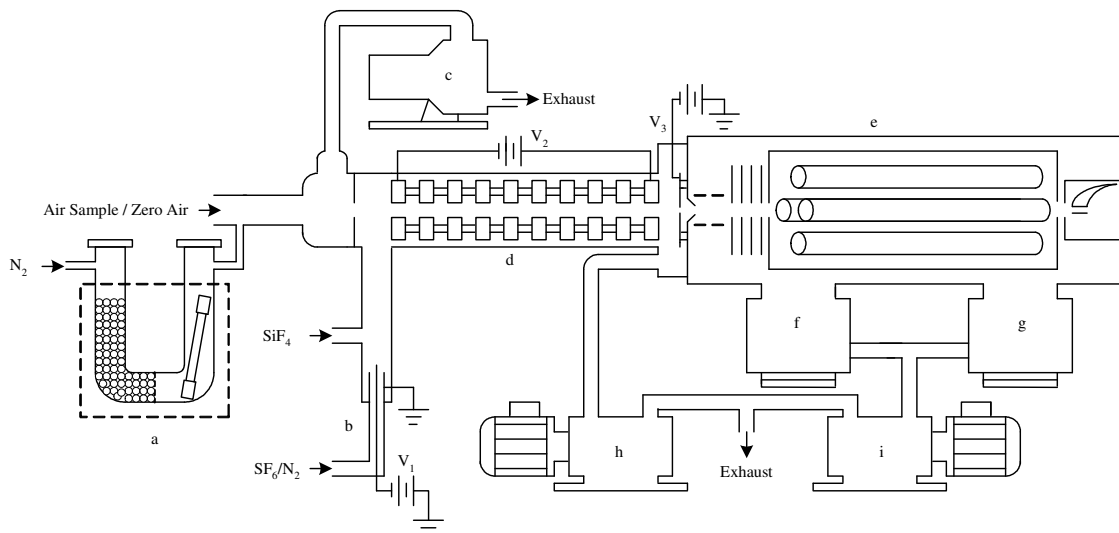


**Fig. 1.** Schematic diagram of the ID-CIMS: **(a)**,  $\text{HNO}_3$  permeation device; **(b)**, ion source; **(c)**, dry scroll pump for air sampling; **(d)**, 10-ring drift tube; **(e)**, Extrel 150-QS mass spectrometer; **(f)** and **(g)**, Varian TV-551 turbo pumps; **(h)**, Edwards E2M30 oil pump; **(i)**, Varian DS402 oil pump.

[Title Page](#)[Abstract](#)[Introduction](#)[Conclusions](#)[References](#)[Tables](#)[Figures](#)[◀](#)[▶](#)[◀](#)[▶](#)[Back](#)[Close](#)[Full Screen / Esc](#)[Printer-friendly Version](#)[Interactive Discussion](#)

Nitric acid during  
MCMA 2006

R. Zhang et al.

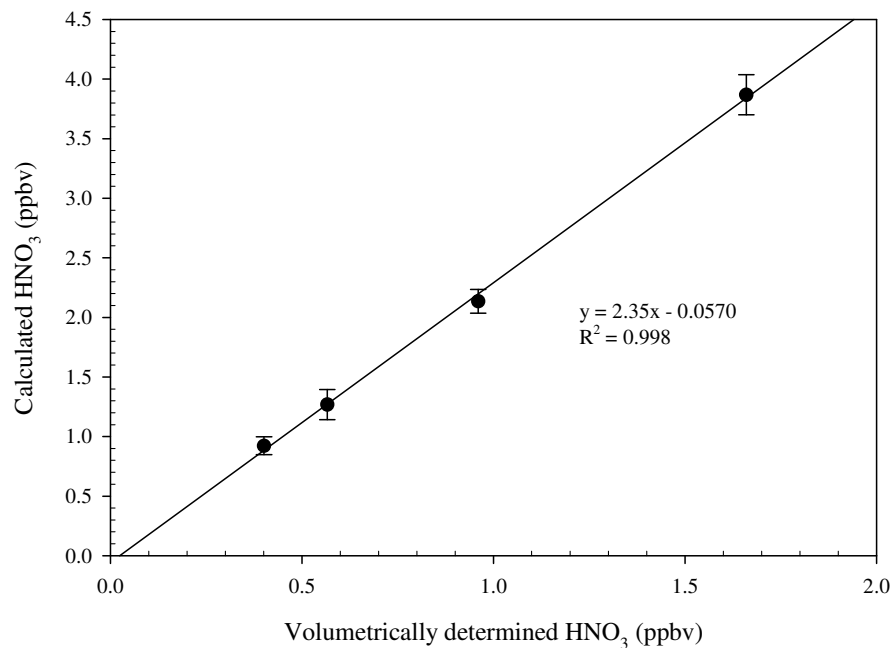


**Fig. 2.** Plot of calculated versus volumetrically prepared HNO<sub>3</sub> concentrations. The slope corresponds to the calibration factor.

[Title Page](#)[Abstract](#)[Introduction](#)[Conclusions](#)[References](#)[Tables](#)[Figures](#)[I◀](#)[▶I](#)[◀](#)[▶](#)[Back](#)[Close](#)[Full Screen / Esc](#)[Printer-friendly Version](#)[Interactive Discussion](#)

Nitric acid during  
MCMA 2006

R. Zhang et al.

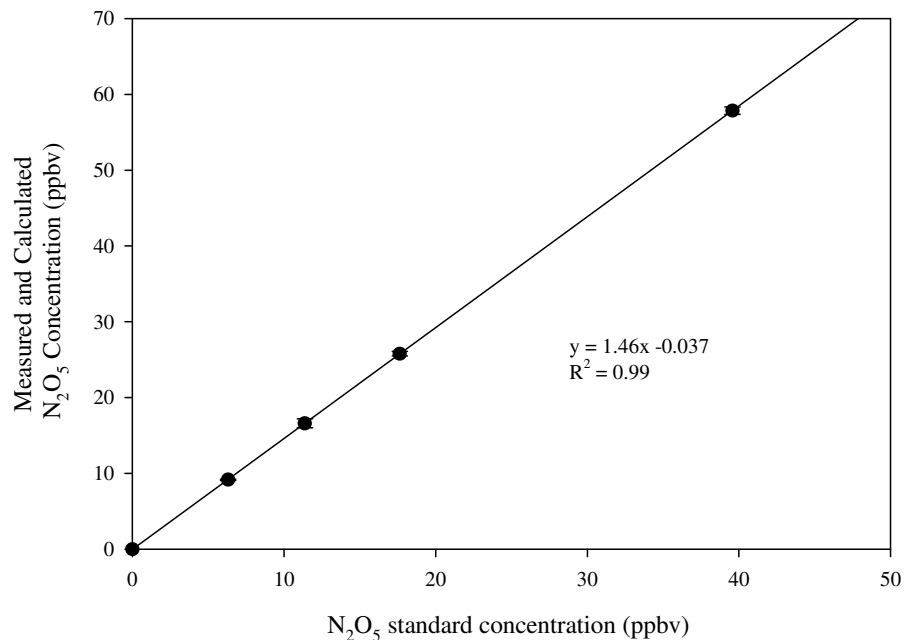


**Fig. 3.** Plot of measured and calculated N<sub>2</sub>O<sub>5</sub> vs. synthesized standards concentration. The slope corresponds to the calibration factor.

[Title Page](#)[Abstract](#)[Introduction](#)[Conclusions](#)[References](#)[Tables](#)[Figures](#)[◀](#)[▶](#)[◀](#)[▶](#)[Back](#)[Close](#)[Full Screen / Esc](#)[Printer-friendly Version](#)[Interactive Discussion](#)

Nitric acid during  
MCMA 2006

R. Zhang et al.

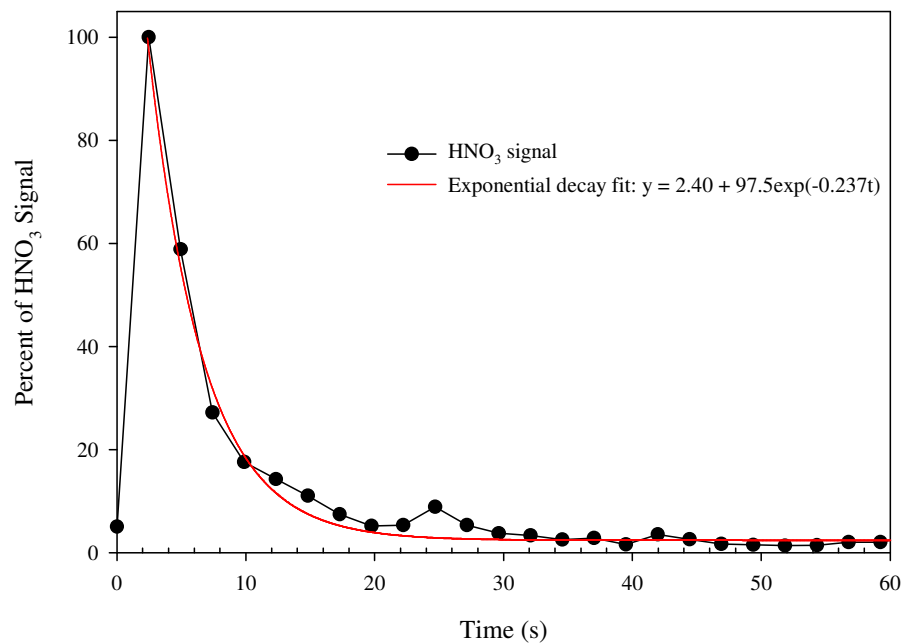


**Fig. 4.** Spike test of the inlet using a 68 wt % HNO<sub>3</sub> solution exposed to the 12 ft inlet for less than one second. The data was collected at 0.4 Hz.

[Title Page](#)[Abstract](#)[Introduction](#)[Conclusions](#)[References](#)[Tables](#)[Figures](#)[◀](#)[▶](#)[◀](#)[▶](#)[Back](#)[Close](#)[Full Screen / Esc](#)[Printer-friendly Version](#)[Interactive Discussion](#)

**Nitric acid during  
MCMA 2006**

R. Zhang et al.

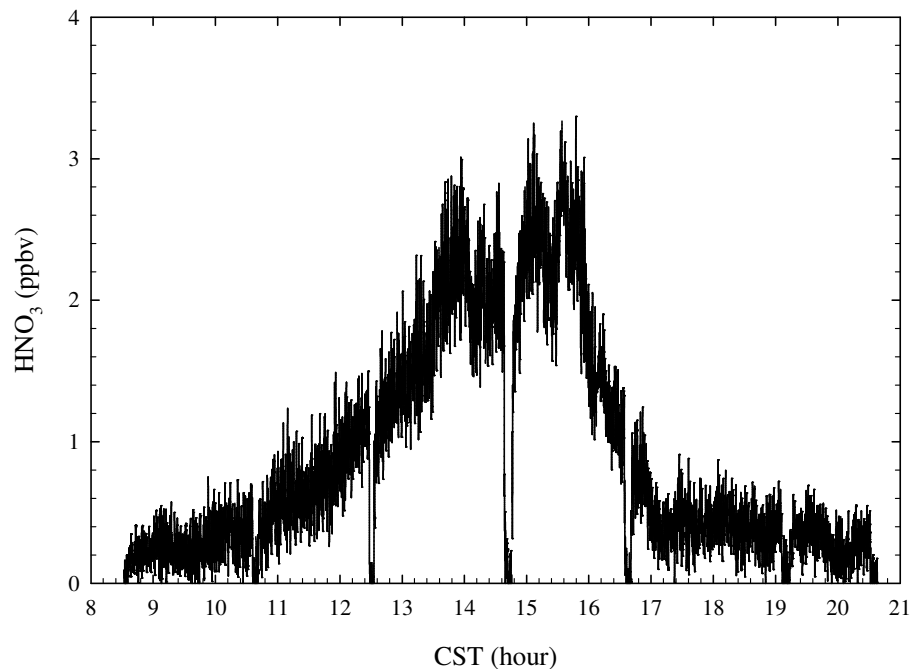


**Fig. 5.** Diurnal profile of HNO<sub>3</sub> observed on 22 March 2006. Backgrounds were checked at 08:36, 10:38, 12:30, 14:39, 16:35, 19:20, and 20:35 CST.

[Title Page](#)[Abstract](#)[Introduction](#)[Conclusions](#)[References](#)[Tables](#)[Figures](#)[I◀](#)[▶I](#)[◀](#)[▶](#)[Back](#)[Close](#)[Full Screen / Esc](#)[Printer-friendly Version](#)[Interactive Discussion](#)

**Nitric acid during  
MCMA 2006**

R. Zhang et al.

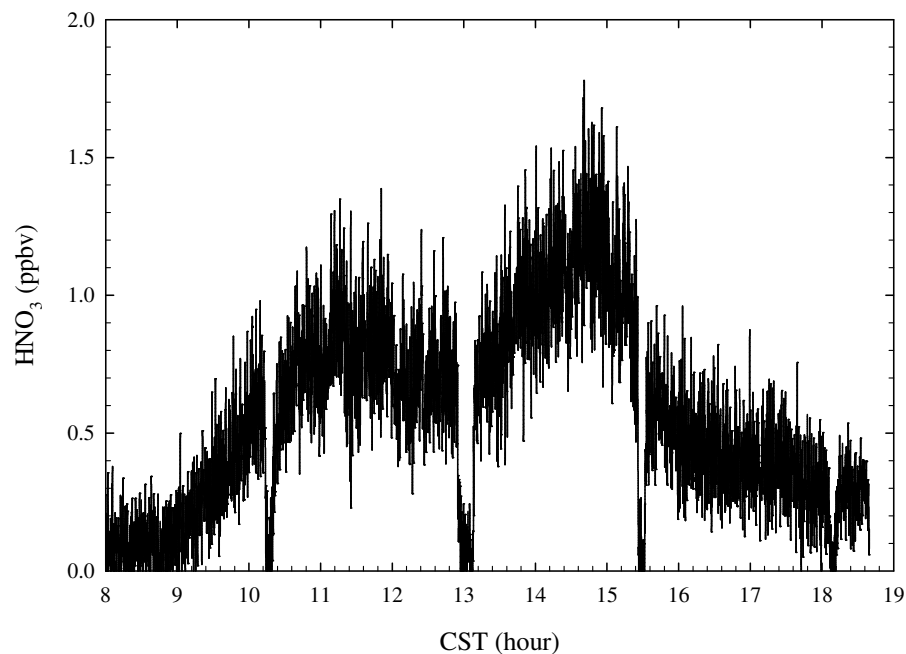


**Fig. 6.** Diurnal profile of HNO<sub>3</sub> observed on 23 March 2006. Backgrounds were checked at 08:00, 10:15, 13:00, 15:30, and 18:10 CST.

[Title Page](#)[Abstract](#)[Introduction](#)[Conclusions](#)[References](#)[Tables](#)[Figures](#)[I◀](#)[▶I](#)[◀](#)[▶](#)[Back](#)[Close](#)[Full Screen / Esc](#)[Printer-friendly Version](#)[Interactive Discussion](#)

Nitric acid during  
MCMA 2006

R. Zhang et al.

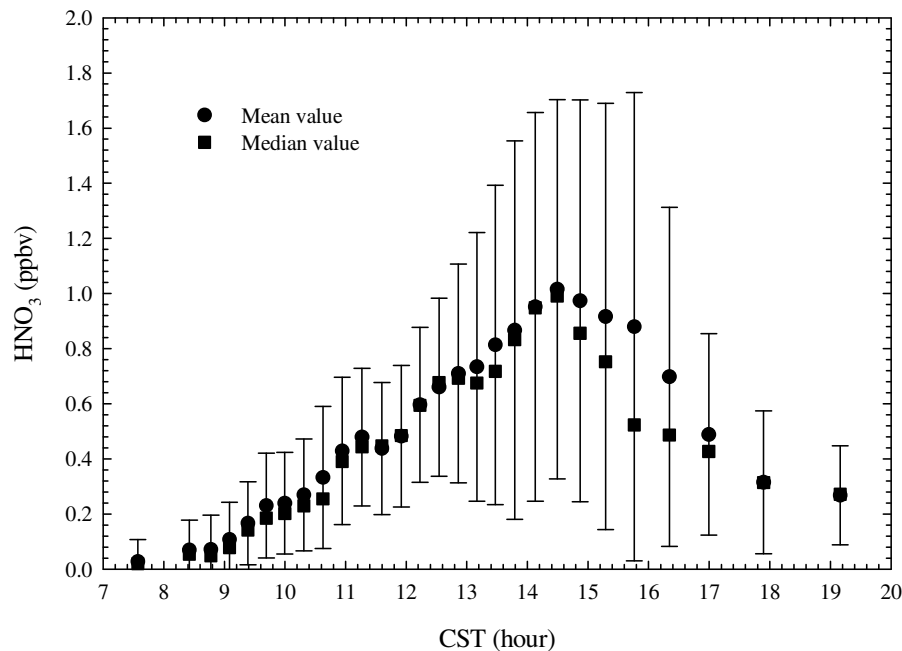


**Fig. 7.** Averaged HNO<sub>3</sub> diurnal profile during the entire field campaign. Each point is based on 1755 data points and the error bars represent one standard deviation.

[Title Page](#)[Abstract](#)[Introduction](#)[Conclusions](#)[References](#)[Tables](#)[Figures](#)[◀](#)[▶](#)[◀](#)[▶](#)[Back](#)[Close](#)[Full Screen / Esc](#)[Printer-friendly Version](#)[Interactive Discussion](#)

Nitric acid during  
MCMA 2006

R. Zhang et al.

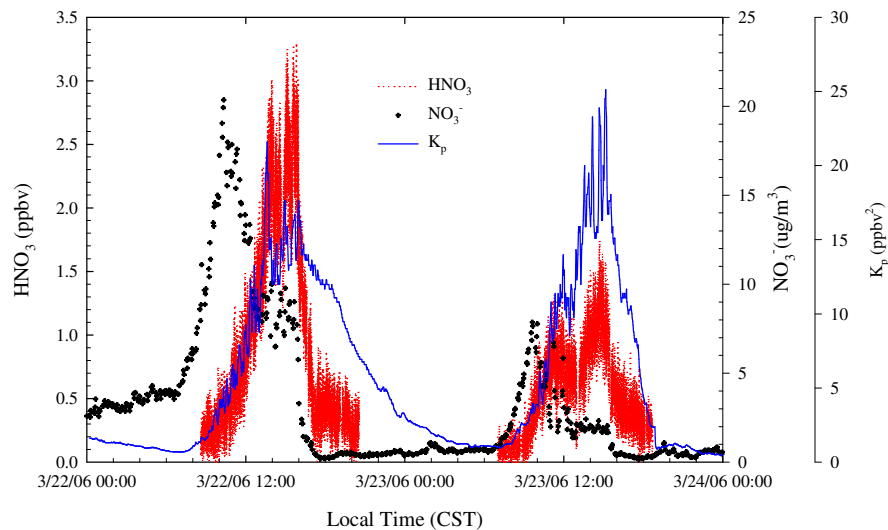


**Fig. 8.** Gaseous  $\text{HNO}_3$ , aerosol nitrate ( $\text{NO}_3^-$ ), and the calculated dissociation constant  $K_p$  of Reaction 18 for 22 and 23 March 2006.

[Title Page](#)[Abstract](#)[Introduction](#)[Conclusions](#)[References](#)[Tables](#)[Figures](#)[◀](#)[▶](#)[◀](#)[▶](#)[Back](#)[Close](#)[Full Screen / Esc](#)[Printer-friendly Version](#)[Interactive Discussion](#)

Nitric acid during  
MCMA 2006

R. Zhang et al.

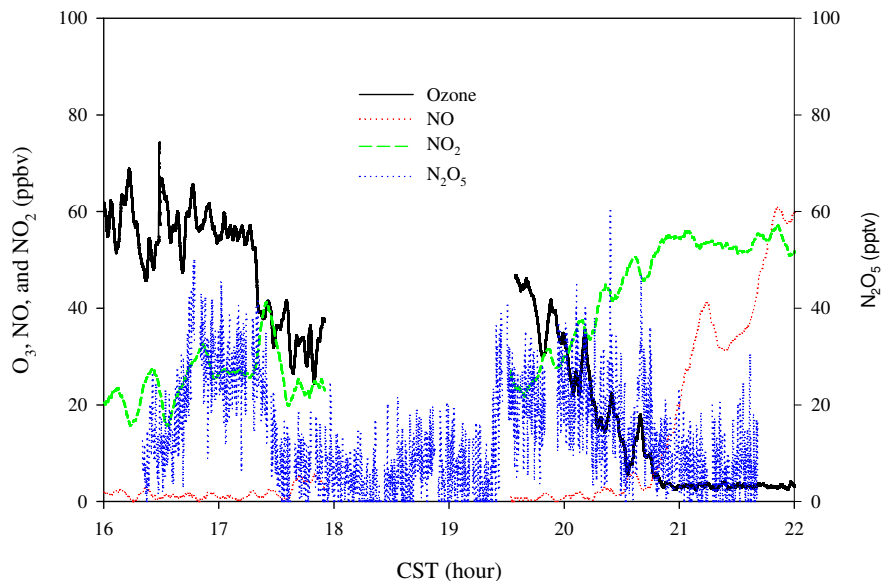


**Fig. 9.**  $\text{N}_2\text{O}_5$  measured on 26 March. Also shown are plots of  $\text{NO}$ ,  $\text{NO}_2$ , and  $\text{O}_3$ . The gap in the measurements was due to instrument calibrations.

[Title Page](#)[Abstract](#)[Introduction](#)[Conclusions](#)[References](#)[Tables](#)[Figures](#)[◀](#)[▶](#)[◀](#)[▶](#)[Back](#)[Close](#)[Full Screen / Esc](#)[Printer-friendly Version](#)[Interactive Discussion](#)

Nitric acid during  
MCMA 2006

R. Zhang et al.

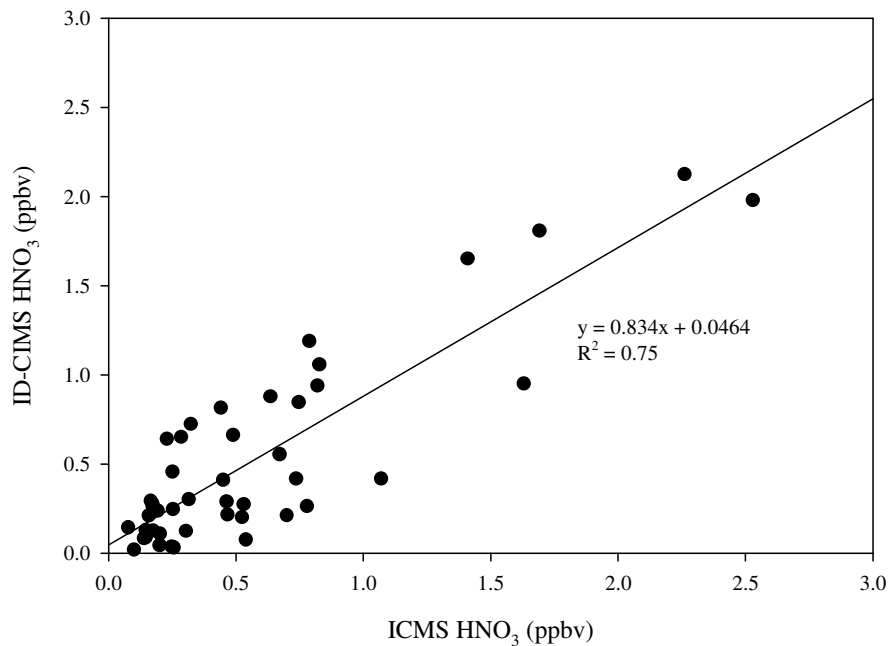


**Fig. 10.** Inter-comparison between the ID-CIMS and ICMS based on 45 overlapping data points collected from 8 to 29 March 2006.

[Title Page](#)[Abstract](#)[Introduction](#)[Conclusions](#)[References](#)[Tables](#)[Figures](#)[I◀](#)[▶I](#)[◀](#)[▶](#)[Back](#)[Close](#)[Full Screen / Esc](#)[Printer-friendly Version](#)[Interactive Discussion](#)